Dielectric Relaxation of Dipole-Inverted Polar Polymers As Studied by Computer Simulations

Yiannis N. Kaznessis, Davide A. Hill, and Edward J. Maginn*

Department of Chemical Engineering, University of Notre Dame, Notre Dame, Indiana 46556

Received April 30, 1999; Revised Manuscript Received July 23, 1999

ABSTRACT: We use molecular dynamics simulations to examine the dielectric relaxation of polar macromolecules with dipoles parallel to the chain backbone. Analysis of the simulation trajectories closely follows the treatment of Watanabe and co-workers for experimental results of dipole-inverted *cis*-polyisoprene solutions (*Macromolecules* **1995**, *28*, 6443). The important observable quantity in experiments and simulations is the dielectric loss spectrum $\epsilon''(\omega)$, whose shape reflects the distribution of relaxation processes for the global chain motion. The observed broadening of the spectra with increasing polymer concentration, classically attributed to overlapping of the chains, is analyzed quantitatively using a local correlation function $C(n,t;m) = 1/a^2 \langle \mathbf{u}(n,t)\cdot\mathbf{u}(m,0)\rangle$, where $\mathbf{u}(n,t)$ is the bond vector of the nth segment of the chain at time t, and $a^2 = \langle \mathbf{u}^2\rangle$. At long times, $C(n,t;m)$ can be expanded as a sum of its eigenmodes: $C(n,t;m) = 2/N\sum_{p=1}^{n} f_p(n)f_p(m)\exp(-t/\tau_p)$, where N is the size of the chain and τ_p and f_p are the relaxation time and the eigenfunction of the pth mode. From simulations we calculate the time correlation functions and dielectric loss spectra of multi-inverted and asymmetrically inverted polar polymers. We compute the relaxation times τ_p and the eigenfunctions of $C(t,n;m)$. The relaxation times follow a power-law dependence $\tau_p \propto p^{-\gamma}$, with $\gamma \simeq 2.08$, and the ratios τ_p/τ_1 remain independent of the concentration, a behavior predicted by the Rouse model. On the other hand, the dependence of f_p on n deviates progressively with increasing density from the Rouse model sinusoidal prediction. The results reveal that the broadening of the spectra is a result of changes in the distribution of eigenmodes (f_p), and not in the relaxation time span γ. Our findings are consistent with the experimental observations, clearly demonstrating the adequacy of simulations for investigating the dynamic behavior of macromolecular systems.

I. Introduction

Dielectric spectroscopy is a powerful tool for examining polymer dynamics.[1,2] Dielectric measurements can reveal information about the global motion of polar polymers. Specifically, type-A polar macromolecules, which possess dipoles parallel to their chain contour,[3] exhibit a slow dielectric "normal-mode" relaxation process.[4]

The main observable experimental quantity is the dielectric loss factor, ϵ''. For chains of N monomers, ϵ'' is tied to the equilibrium autocorrelation function of the chain end-to-end vector, $\phi_0(t)$, through

$$\epsilon''(\omega)/\Delta\epsilon = \int_0^\infty \left[-\frac{\mathrm{d}\phi_0(t)}{\mathrm{d}t}\right] \sin(\omega t)\mathrm{d}t \tag{1}$$

where $\Delta\epsilon$ is the dielectric intensity for the global chain motion, and

$$\phi_0(t) = \frac{\langle \mathbf{R}(0)\cdot\mathbf{R}(t)\rangle}{\langle \mathbf{R}(0)\cdot\mathbf{R}(0)\rangle} \tag{2}$$

with $\mathbf{R} = \mathbf{r}_N - \mathbf{r}_1$. The brackets in eq 2 indicate ensemble averages. A detailed picture of the dynamics of polymer chains emerges by identifying a local correlation function.[5−7]

$$C(n,t;m) = \frac{1}{a^2}\langle \mathbf{u}(n,t)\cdot\mathbf{u}(m,0)\rangle \tag{3}$$

where $\mathbf{u}(n,t)$ is the bond vector of the nth chain segment at time t, and $a^2 = \langle \mathbf{u}^2\rangle$. The correlation function $\phi_0(t)$ can then be written in terms of $C(n,t;m)$ as

$$\phi_0(t) = \frac{1}{N}\int_0^N \mathrm{d}n \int_0^N \mathrm{d}m C(n,t;m) \tag{4}$$

$C(n,t;m)$ can be expanded at long times with respect to its eigenfunctions f_p ($p = 1,...,N$) as;[5−7]

$$C(n,t;m) = \frac{2}{N}\sum_{p=1}^{N} f_p(n)f_p(m)\exp(-t/\tau_p) \tag{5}$$

where the relaxation time τ_p is calculated as the inverse of the pth eigenvalue. The functional form of $f_p(n)$ and the span of relaxation times τ_p with p determine the character of the chain dynamical behavior. Using eqs 1, 4, and 5 the dielectric loss can be written as

$$\epsilon''(\omega)/\Delta\epsilon = \sum_{p=1}^{N} g_p(N)\frac{\omega\tau_p}{1+\omega^2\tau_p^2} \tag{6}$$

where the intensity of the pth dielectric mode is given by

$$g_p(N) = \frac{2}{N^2}\left(\int_0^N f_p(n)\,\mathrm{d}n\right)^2 \tag{7}$$

One of the most intriguing experimental observations is the broadening of the dielectric mode distribution with increasing concentration, as seen in the shape of $\epsilon''(\omega)$. Patel and Takahashi[8] and Urakawa et al.[9] measured the dielectric loss for *cis*-polyisoprene (PI), a type-A polymer, in solutions of good solvents and found that the spectra become broader with increasing concentra-

10.1021/ma990680u CCC: $18.00
Published on Web 09/09/1999

tion. They attributed this behavior, in phenomenological terms, to overlapping of the chains. Theoretically, for unentangled chains the Rouse model predicts that $f_p(n) \propto \sin(p\pi n/N)$ and $\tau_p \propto p^{-2}$ regardless of the concentration,[10] so that ϵ'' can be written as

$$\epsilon''(\omega)/\Delta\epsilon = \frac{8}{\pi^2}\sum_{p=1}^{N}\frac{\omega\tau_p}{p^2(1+\omega^2\tau_p^2)} \qquad (p\text{: odd}) \qquad (8)$$

The Rouse model does not account for hydrodynamic interactions (HI), which play an important role for dilute and semidilute solutions. The Zimm model[11] does account for HI, but its mode distribution is identical with that of the Rouse model. There is a small difference between the two theories in the τ_p dependence on p, but it only results to minor deviations of the spectra at high frequencies. For entangled chains the reptation model also predicts the same mode distribution as the Rouse model. Consequently, the theoretical predictions are inconsistent with experimental observations, because they suggest that the dielectric loss curves have the same shape, regardless of the concentration.

Urakawa et al.[14] suggested that the broadening is caused by changes in the span of τ_p with increasing concentration c, as predicted by Muthukumar's relation (15):

$$\tau_p = \tau_{p,0}[1 + cAp^{-\kappa} - 2^{0.5}(cAP^{-\kappa})^{1.5} + 2(cAP^{-\kappa})^2 + ...] \quad (9)$$

where $\tau_{p,0}$ is the relaxation time of the pth mode at infinite dilution, A is a constant proportional to the intrinsic viscosity $[\eta]$, and $\kappa = 3\nu - 1$, ν being the Flory coefficient of polymer dimensions.[16] Recently, however, Urakawa and Watanabe[17] concluded that the broadening is not caused by changes in τ_p, as Muthukumar's theory suggests. Rather, they concluded that the broadening is a result of changes in the dielectric intensity distribution ratio g_p/g_1, caused by changes in the n dependence of $f_p(n)$. These authors based their conclusion on dielectric spectroscopy measurements of once-inverted PI chains.[5−7] Specifically, Watanabe and coworkers were able to calculate the relaxation times τ_p and the eigenfunctions $f_p(n)$ for $p = 1,2,3$ for solutions of different PI concentration and identify the reason of the dielectric spectra broadening in terms of changes in the eigenfunctions, f_p. A summary of their treatment of the experimental results is given in the Appendix.

Although these experiments provided a breakthrough in understanding the mechanisms of global chain motion, they have been limited to only the first three eigenfunctions and relaxation times, with the estimation accuracy for the third mode being rather limited.[5] More detailed analysis would require chains twice-inverted to accurately calculate τ_3 and $f_3(n)$. It would further require chains inverted three or more times to calculate relaxation times and eigenfunctions for $p \geq 4$. Such dielectrically labeled chains are hard to synthesize, however, so that one would have to resort to other methodologies.

Computer simulations represent an important means for integrating experimental findings and theoretical hypotheses. We previously have used molecular dynamics simulations to study the dielectric relaxation of type-A polar macromolecules in good solvents[18,19] and in θ solvents.[20] The same behavior of the dielectric loss was observed in the simulation results as in the experiments, namely broadening with increasing concentration. A normal-mode analysis revealed that the mode correlation functions deviate progressively from the theoretical prediction of the Rouse/reptation models with increasing concentration and molecular weight, resulting into broader dielectric loss spectra. From this analysis, however, no definite conclusions can be drawn about the role of the ratios τ_p/τ_1 and g_p/g_1. In this article, we analyze the results of the simulation trajectories in terms of local correlation functions and calculate relaxation times τ_p and eigenfunctions $f_p(n)$ for $p \leq 6$, complementing and clarifying in microscopic terms the experimental findings of Watanabe et al. In addition to the microscopic insight that simulations provide, they enable monodisperse systems of purely type-A polar chains to be examined. Consequently, simulation results are not subject to considerations of effects, such as the molecular weight distribution and the segmental mode dielectric relaxation. These factors significantly influence the experimental loss spectra shapes.

The rest of the article is organized as follows. First, the fundamental characteristics of the simulations are described. Next, the transient dielectric response of multi-inverted macromolecules (type-A chains with two or more dipole inversions) is shown to be given by the correlation function of equilibrium fluctuations of corresponding chain segments. Then, the dielectric spectra of multi-inverted chains, with up to five inversions, are presented and the relaxation times τ_p for $p \leq 6$ are calculated for all the systems simulated in refs 18 and 19. In the next section, the dielectric spectra of asymmetrically inverted chains are presented, and the eigenfunctions are calculated for different parts of the chains and compared with theoretical predictions.

II. Simulation Methodology

Because the details of the simulation methodology have been described in refs 18 and 19, we only summarize the characteristics of the systems studied. A bead-spring model was used to simulate chains of N monomers ($50 \leq N \leq 150$) at different bead number densities ρ ($0.0 \leq \rho \leq 0.80$). The important parameters used in the simulations are the size of the beads σ, the mass of the beads m, the parameter ϵ for the interaction potentials, and the reduced simulation time $\tau = \sigma(m/\epsilon)^{1/2}$. The solvent is not considered explicitly. Instead, the beads are considered to be immersed in a heat bath which provides thermal energy that is viscously dissipated. Hydrodynamic interactions (HI) are not taken into account, resulting in quantitative deviations between the simulation and the experimental scaling of dynamic properties at low concentrations. Increasing the concentration, HI are screened out and the simulations capture accurately the behavior of real systems.

Equilibrium systems in a good solvent were mainly studied. Nonequilibrium simulations, used when necessary, enabled the response of the chains to external electric fields to be computed. In the nonequilibrium simulations the chains were modeled as type-A polar polymers, by adding partial charges at the center of mass of the end beads, but no electrostatic interactions were taken into account between different chains in the equilibrium (no electric fields) and the nonequilibrium simulations. The electric fields, which are coupled with the charges in the nonequilibrium simulations, produce responses in the linear regime.[18]

Crossover densities, demarcating the onset of chain overlap, were estimated for different chain sizes as $\rho_{50}^* = 0.030$, $\rho_{100}^* = 0.017$, and $\rho_{150}^* = 0.012$.[18] For densities $\rho \leq \rho^*$, the dielectric spectra are very close to the theoretical prediction of the Rouse model. For $\rho > \rho^*$, however, the spectra broaden considerably with increasing concentration when in the nonentangled

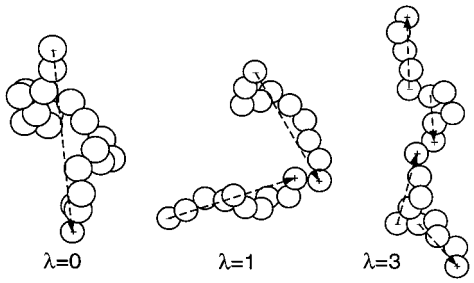

Figure 1. Schematic illustration of symmetrically multi-inverted polar chains with λ points of inversion.

regime. When entanglements set in, the main peak does not broaden any further, but a secondary peak appears at the high-frequency side of the spectrum.[19]

III. Results

III-1. Dielectric Response of Multi-inverted Dipoles. In ref 18, we demonstrated that the transient response of type-A polar chains under the influence of external electric fields is congruent with the time autocorrelation function of the end-to-end vector at equilibrium. In this section, we show that the response of symmetrically multi-inverted (with λ points of inversion) polar chains to external electric fields can be given by the time autocorrelation functions of the corresponding chain segments at equilibrium. For illustrative purposes, Figure 1 shows polar chains with no dipole inversion ($\lambda = 0$), with one ($\lambda = 1$) and with three ($\lambda = 3$) dipole inversions. Chains with up to five inversions have been used in the present study.

Applying an electric field E to systems with chains of size $N = 30$ at a density $\rho = 0.5$, inverted λ times ($0 \leq \lambda \leq 4$), we monitor the buildup of the polarization. Once a system reaches the steady state, the electric field is turned off at time $t = 0$, and the normalized decay of the polarization $a(t)$ is monitored. $a(t)$ is given by $a(t) = |\Delta\mathbf{P}(t)|/|\Delta\mathbf{P}(0)|$, where $\Delta\mathbf{P}(t) = \mathbf{P}(t) - \langle\mathbf{P}\rangle_0$ is the departure of the polarization $\mathbf{P}$ from its equilibrium value $\langle\mathbf{P}\rangle_0$. The polarization is calculated as the vectorial sum of all the dipoles in the system divided by the volume of the system. For homogeneous solutions $\langle\mathbf{P}\rangle_0 = 0$. The electric field strength and the partial charges are the same as in ref 18. Independently, an equilibrium simulation is performed at the same state point, but with no electrostatic interactions. From the equilibrium trajectories, the segmental correlation functions that correspond to the transient response of polar chains with λ inversions are computed as

$$\phi_\lambda(t) = \frac{\langle\Psi(0)\cdot\Psi(t)\rangle}{\langle\Psi(0)\cdot\Psi(0)\rangle} \tag{10}$$

where

$$\Psi(t) = \sum_{i=1}^{\lambda}(-1)^{i+1}[\mathbf{r}_{iN/(\lambda+1)}(t) + \mathbf{r}_{iN/(\lambda+1)+1}(t)] - \mathbf{r}_1(t) + (-1)^{\lambda}\mathbf{r}_N(t) \tag{11}$$

In Figure 2, the normalized decay functions $a_\lambda(t)$ obtained from the nonequilibrium response of systems with polar chains inverted symmetrically λ times ($0 \leq \lambda \leq 4$) are plotted versus time. Also plotted in Figure 2 are the equilibrium correlation functions ϕ_λ. This plot demonstrates the congruence of the transient responses to the correlations of equilibrium fluctuations. It also becomes clear that only one equilibrium simulation is required to obtain the response for all values of λ, whereas separate nonequilibrium simulations must be conducted for different values of λ. Therefore, we resort to equilibrium simulations to calculate ϕ_λ.

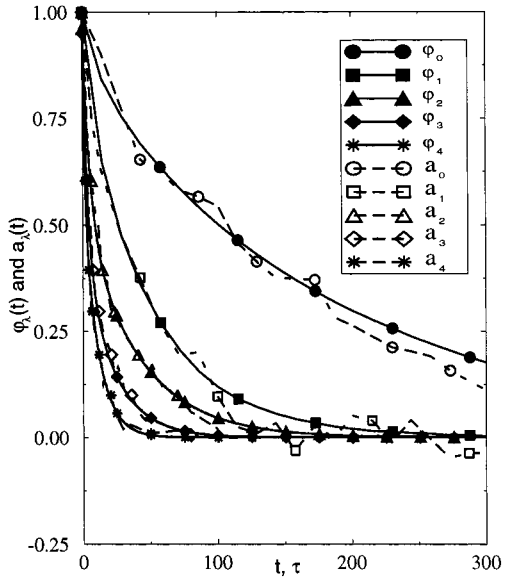

Figure 2. Equilibrium correlation functions $\phi_\lambda(t)$ and transient response normalized decay functions $a_\lambda(t)$ for chains with $N = 30$ at $\rho = 0.5$.

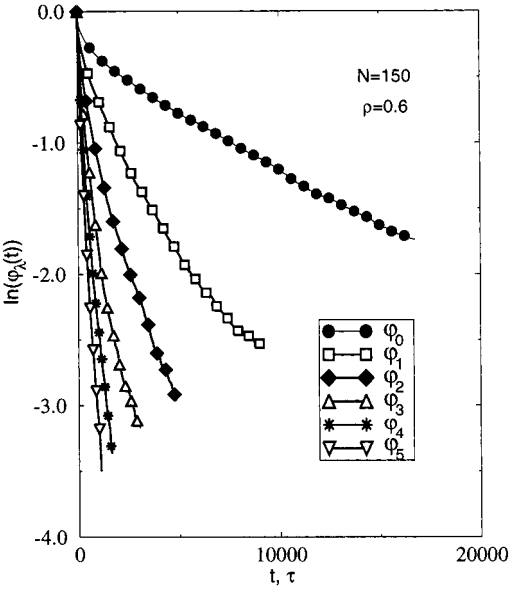

Figure 3. Correlation functions $\phi_\lambda(t)$ with $N = 150$ chains with λ inversions at $\rho = 0.6$.

III-2. Dielectric Loss Spectra for Multi-inverted and Asymmetrically Inverted Polar Chains. From previous equilibrium simulation trajectories,[18,19] we calculate the correlation functions ϕ_λ, $\lambda \leq 5$. In Figure 3 we plot ϕ_λ for the system with chains of size $N = 150$ at a reduced density $\rho = 0.6$. The correlation functions decay faster with an increasing number of inversion points. This is expected, because they describe fluctuations of smaller chain segments. At long time scales, ϕ_λ apparently decay as single exponentials. There is some curvature at small times, however, indicating a distribution of relaxation processes.

Taking the Laplace−Fourier transform of $\phi_\lambda(t)$ yields the reduced dielectric loss $E''(\omega, \lambda) = \epsilon''(\omega, \lambda)/\Delta\epsilon$. In Figure 4, $E''(\omega, \lambda)$ is plotted as a function of frequency

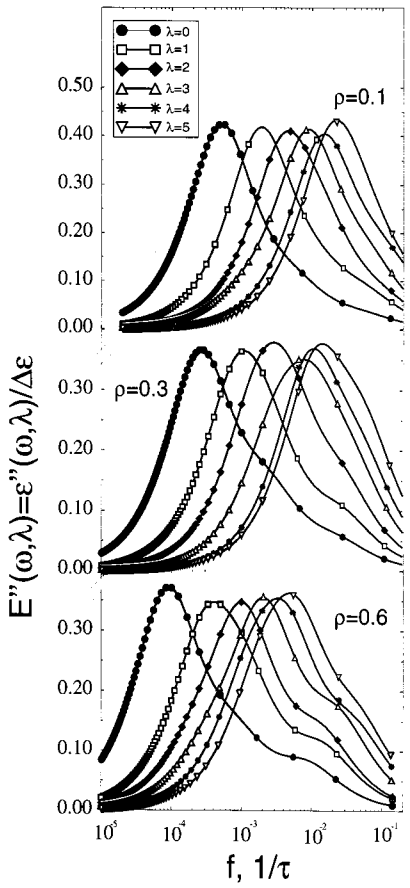

Figure 4. Frequency dependence of the normalized dielectric loss $\epsilon''(\omega,\lambda)/\Delta\epsilon$ for multi-inverted chains of $N = 150$ at densities ρ.

f for systems with chains of $N = 150$ at densities $\rho = 0.1$, 0.3, and 0.6.

With increasing density the spectra for $\lambda = 0$ broaden considerably, displaying relaxation behavior different than that predicted theoretically. The most notable discrepancy occurs for $\rho = 0.6$, where a bimodal distribution of relaxation times becomes apparent, as evidenced by the weak shoulder at $f \simeq 7 \times 10^{-3}$. In refs 18 and 19, the broadening was attributed to chain overlapping, and the secondary peak appearing at high frequencies for the dense systems was explained as a result of entanglements. With an increasing number of inversions, the spectra shift to higher frequencies. It can be observed that the shape of the loss curves remains almost identical for $\lambda = 0$ and $\lambda = 1$. This feature also was observed experimentally by Watanabe et al.[5,7] It seems, however, that there is a gradual change of the distribution of relaxation processes with increasing λ. This change is clearer in the plot for the systems at $\rho = 0.6$. We have calculated the dielectric loss curves for all the systems studied in refs 18 and 19 and have found that the spectra tend to the distribution of the Rouse model, given by eq 8, for numerous inversions.

The effect of the location of the inversion point on the dielectric loss spectra can also be examined. The correlation function $\phi_{n^*}(t)$ is defined as

$$\phi_{n^*}(t) = \{\langle(\mathbf{r}_N(t) - \mathbf{r}_{n^*+1}(t) - \mathbf{r}_{n^*}(t) + \mathbf{r}_1(t))\cdot(\mathbf{r}_N(0) - \mathbf{r}_{n^*+1}(0) - \mathbf{r}_{n^*}(0) + \mathbf{r}_1(0))\rangle\}/\{\langle(\mathbf{r}_N(0) - \mathbf{r}_{n^*+1}(0) - \mathbf{r}_{n^*}(0) + \mathbf{r}_1(0))\cdot(\mathbf{r}_N(0) - \mathbf{r}_{n^*+1}(0) - \mathbf{r}_{n^*}(0) + \mathbf{r}_1(0))\rangle\} \quad (12)$$

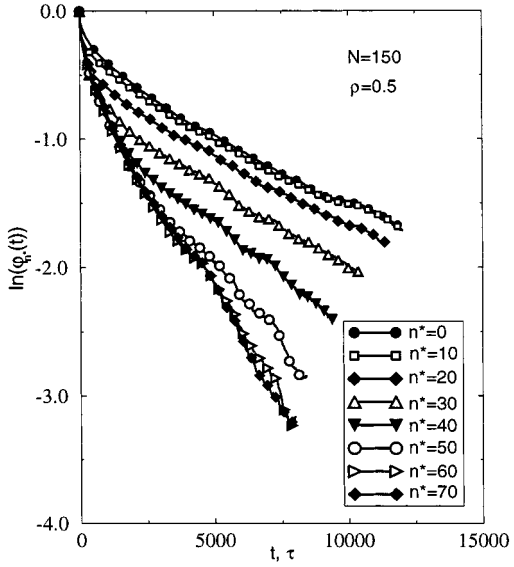

Figure 5. Time dependence of the correlation functions $\phi_{n^*}(t)$ of $N = 150$ chains at $\rho = 0.5$ inverted once at n^*.

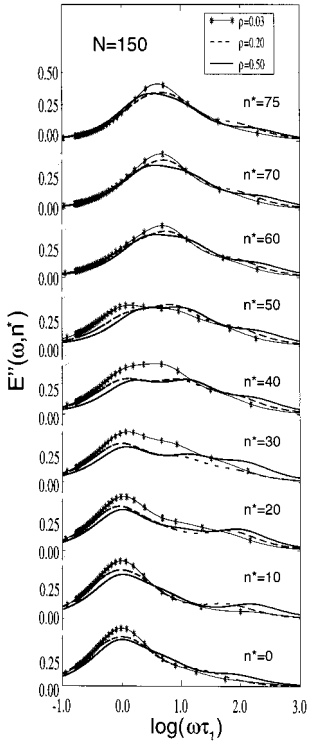

Figure 6. Dielectric loss spectra $E''(\omega,n^*)$ of once-inverted $N = 150$ chains at different densities ρ.

where n^* defines the location of a single inversion point along the chain backbone. $\phi_{n^*}(t)$ was computed for $n^* =$ 0,10,20,30,40,50,60,70,75 for chains with $N = 150$. Figure 5 shows $\phi_{n^*}(t)$ for chains of size $N = 150$ at $\rho = 0.5$. At small time scales $\phi_{n^*}(t)$ decays in the same fashion for all n^*, with the embedded relaxation of small chain pieces dominating. At longer time scales the curves start separating, with the relaxation mechanism of larger segments dominating $\phi_{n^*}(t)$.

Taking the Laplace−Fourier transform of these correlation functions yields the reduced dielectric loss $E''(\omega,n^*)$. The loss spectra are presented in Figure 6 versus a reduced frequency $\omega\tau_1$ for chains with $N = 150$ at three different densities $\rho = 0.03$, 0.20 and 0.50. Remarkably different dielectric behavior is observed by

Table 1. Relaxation Times τ_p ($p = 1-6$) for Systems of Chains with size $N = 150$ at Densities ρ

N	ρ	τ_1	τ_2	τ_3	τ_4	τ_5	τ_6
150	0.01	1650	390	155	88	55	35
150	0.03	1710	410	159	95	61	40
150	0.10	2082	520	200	110	70	48
150	0.20	2454	660	270	145	80	55
150	0.30	3844	890	360	200	130	78
150	0.40	5245	1300	505	310	174	125
150	0.50	8410	2150	870	460	295	210
150	0.60	10950	2600	1200	590	370	280
150	0.70	17660	4100	1700	980	600	440
150	0.80	34450	8450	3400	1990	1220	850

moving the inversion point from the end to the middle of the chains. As the inversion point moves toward the middle of the chain, the spectra broaden reaching clear multimodal shapes for $n^* = 20-40$. They subsequently narrow almost to the shape of noninverted chains at about $n^* = 60$. The main peaks occur at higher frequencies with increasing n^*, indicating shorter relaxation times. All these observations are consistent with experimental observations.[5-7]

III-3. Relaxation Time τ_p Dependence on p and ρ. The relaxation times τ_p, $p \leq 6$, where τ_1 is the relaxation time of noninverted chains ($\lambda = 0$), τ_2 is the relaxation time of chains inverted once at $n^* = N/2$ ($\lambda = 1$), etc., can be calculated as the inverse frequency of the maximum dielectric loss, shown in Figure 4. This calculation rests on the assumption of zero dielectric intensities for all the ith eigenmodes ($i \neq p$). This is indeed true for $p = 1$, 2, because of the symmetry of these eigenfunctions (see the Appendix). As mentioned in the Introduction, the Rouse model predicts a sinusoidal dependence of the eigenfunctions f_p with n. In this case, the symmetry of the eigenfunctions leads to zero dielectric intensities for $i \neq p$ and the relaxation time τ_p can be calculated accurately as the inverse frequency of the maximum dielectric loss. For the simulated chains, however, a progressive deviation from the theoretical behavior is observed (see next section). This deviation might lead to nonzero contributions of slower eigenmodes with $i < p$ in the low-frequency tail of the dielectric loss curves. Nevertheless, the loss peaks of λ symmetrically inverted polar chains will still be dominated by the $p = \lambda + 1$ eigenmode and the peak frequency accurately gives τ_p for the chains simulated in this work. In Table 1, we list the relaxation times for all the simulated systems with $N = 150$.

In Figure 7, the dependence of τ_p on p is shown for systems with $N = 150$ at different densities. The plot clearly demonstrates a power-law relationship, $\tau_p \propto p^{-\gamma}$. The reptation and the Rouse models predict such a relationship, with $\gamma = 2$. The slopes $-\gamma$ in the plot are very close to the theoretical prediction. The small deviation can be explained in terms of excluded volume effects, not considered in the Rouse theory. Experimentally,[7] γ varied from 1.75 to 1.95 for PI concentrations ranging from dilute ($c_{PI} = 0.027$ g cm^{-3}) to melt (0.92 g cm^{-3}). The difference between the simulation and the experimental γ is likely caused by the neglect of hydrodynamic interactions in the simulation model. With increasing concentration, the experimental results approach the simulation ones, because of screening of hydrodynamic and excluded volume effects.

Another point that can be deduced from the plot is that there is no change in the span of relaxation times with increasing density. Therefore, we can speculate

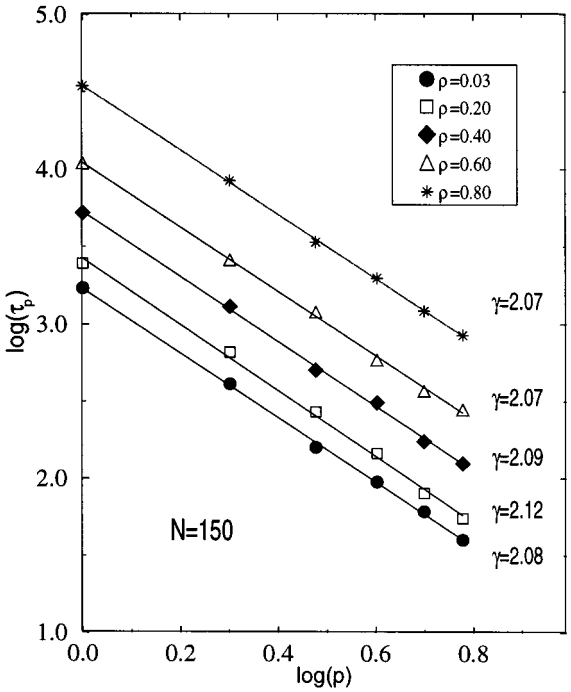

Figure 7. Relaxation times τ_p dependence on the number of the mode p for $N = 150$ chains at densities ρ. The evaluated slopes indicate a power−law relationship, $\tau_p \propto p^{-\gamma}$.

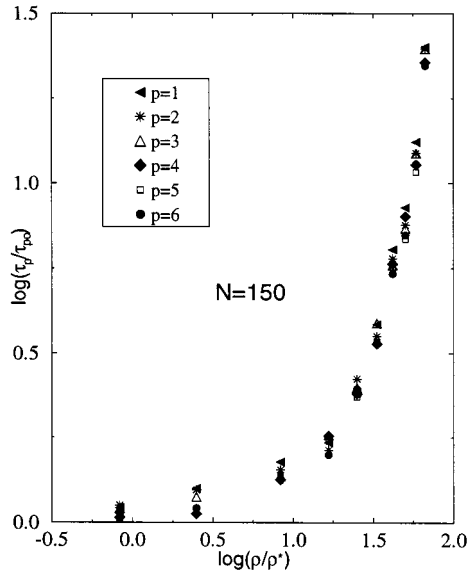

Figure 8. Ratio of relaxation times $\tau_p/\tau_{p,0}$ for $p = 1-6$ as function of reduced density ρ/ρ^*.

that the change in the experimental power law is due to the screening of hydrodynamic effects.

The effect of density on the relaxation times τ_p is illustrated in Figure 8. The reduced relaxation times $\tau_p/\tau_{p,0}$, where $\tau_{p,0}$ is the pth mode relaxation time at infinite dilution, are plotted versus the reduced density ρ/ρ^* for $N = 150$ and $1 \leq p \leq 6$. The ratio ρ/ρ^* is a measure of chain overlapping.

Increasing the concentration, the ratio $\tau_p/\tau_{p,0}$ increases significantly. It is observed that the increase is almost identical for all the modes p, a feature observed in the experiments by Watanabe and co-workers, for $p = 1$, 2, 3. This rapid increase was attributed by Watanabe and co-workers[7] partly to entanglement effects. However, this behavior persists for higher modes that describe

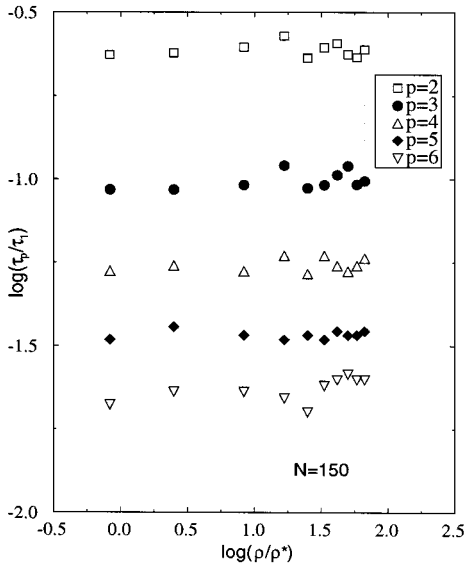

Figure 9. Dependence of τ_p/τ_1 on reduced density ρ/ρ^* for $N = 150$ chains.

the relaxation of segments smaller than the entanglement length (for this model, $N_e \simeq 35$, at $\rho = 0.85$, ref 21). Therefore, one is led to the conclusion that the increase in relaxation times with density is a result of the rapid increase in the effective friction coefficient that slows down the chain motion. However, one has to consider that such a conclusion is based on the perception that the higher modes with characteristic lengths $N < N_e$ are not affected by entanglement effects. The reptation theory does not account for a spatial cutoff for the entanglement effects, although it is not clear whether, in real dynamics, entanglements influence the behavior of chain segments smaller than the entanglement length.

As Watanabe et al. point out, Muthukumar's theory accounts neither for entanglement effects nor the increase of the friction factor, suggesting a less pronounced increase of the ratio $\tau_p/\tau_{p,0}$ for the higher modes. Figure 8 indicates a behavior close to the experimental one, that cannot be reconciled by the theory. In addition, Muthukumar's theory as summarized in eq 9 predicts that the ratio τ_p/τ_1 depends on the concentration. Specifically, at low concentrations τ_p/τ_1 is essentially constant, but when the chains begin overlapping τ_p/τ_1 decreases considerably, reaching a new plateau at very high concentrations. Watanabe et al.[7] computed that at a concentration $c_{PI} = 4c^*$, where c^* is the crossover concentration, the model predicts $\tau_2/\tau_1 = 0.194$ and $\tau_3/\tau_1 = 0.079$, whereas the experimental ratios are $\tau_2/\tau_1 = 0.269$ and $\tau_3/\tau_1 = 0.143$.

In Figure 9 we show in a double logarithmic plot the ratio τ_p/τ_1 versus the reduced density ρ/ρ^*. As in the experiments, the ratios τ_p/τ_1 appear to be independent of the density, with average values $\tau_2/\tau_1 \simeq 0.244$, $\tau_3/\tau_1 \simeq 0.1$, $\tau_4/\tau_1 \simeq 0.055$, $\tau_5/\tau_1 \simeq 0.034$, and $\tau_6/\tau_1 \simeq 0.023$. Thus it appears that both simulations and experiments give a concentration dependence for τ_p/τ_1 that differs from Muthukumar's theory.

III-4. Local Correlation Eigenfunctions $f_p(n)$. From our simulations, we have calculated the correlation functions $\phi_1(t,n^*)$ using eq 12. We have followed closely the treatment by Watanabe et al.[5−7] described in the Appendix, allowing a direct comparison of experimental and simulation results. From eqs A1, 5, and A7 it follows that

$$\phi_1(t,n^*) = \sum_{p=1}^{N} [2\Delta F_p(n^*)]^2 \exp(-t/\tau_p) \qquad (13)$$

Assuming that the sum in eq 13 for $p \geq 7$ is negligible, and with the relaxation times τ_p already computed, $\Delta F_p(n^*)$ can be obtained through use of a least-squares analysis.

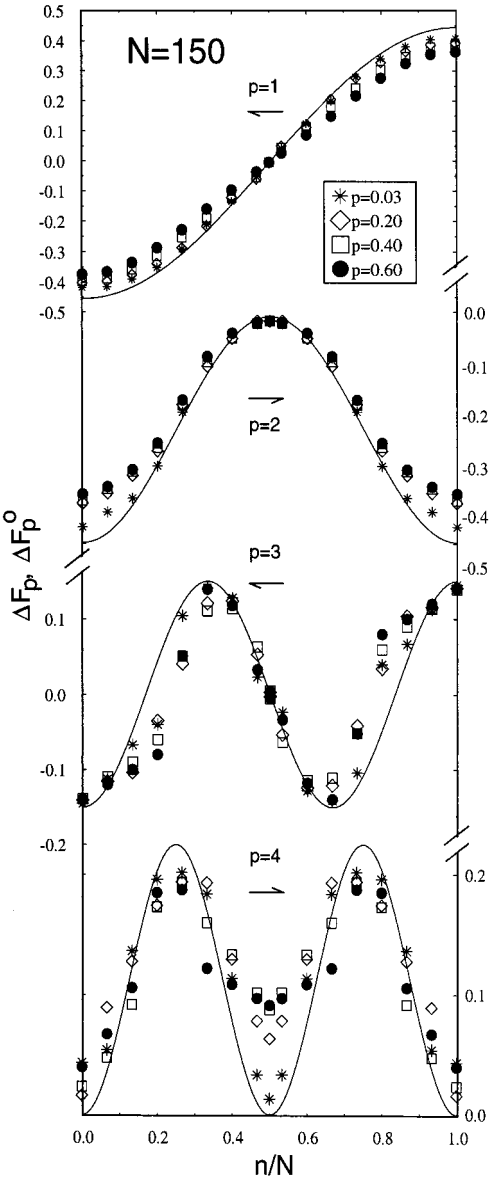

Figure 10. Eigenfunctions $\Delta F_p(n)$ ($p = 1-4$) against n/N for $N = 150$ chains at densities ranging from 0.03 to 0.60. The solid lines are $\Delta F_p^o(n)$ predicted by theories and computed using eq 14.

In Figure 10, $\Delta F_p(n)$ for $p = 1-4$ is plotted as a function of the ratio n/N for $N = 150$ at different densities. The solid lines in Figure 10 are the Rouse−Zimm model and the reptation model predictions for $\Delta F_p(n)$. These models predict a sinusoidal dependence of the eigenfunctions on n in the form of $f_n^o(n) = \sin(p\pi n/N)$. Therefore, one obtains

$$\Delta F_p^o(n) = \frac{\sqrt{2}}{p\pi}\left[\cos\frac{p\pi}{2} - \cos\frac{p\pi n}{N}\right] \qquad (14)$$

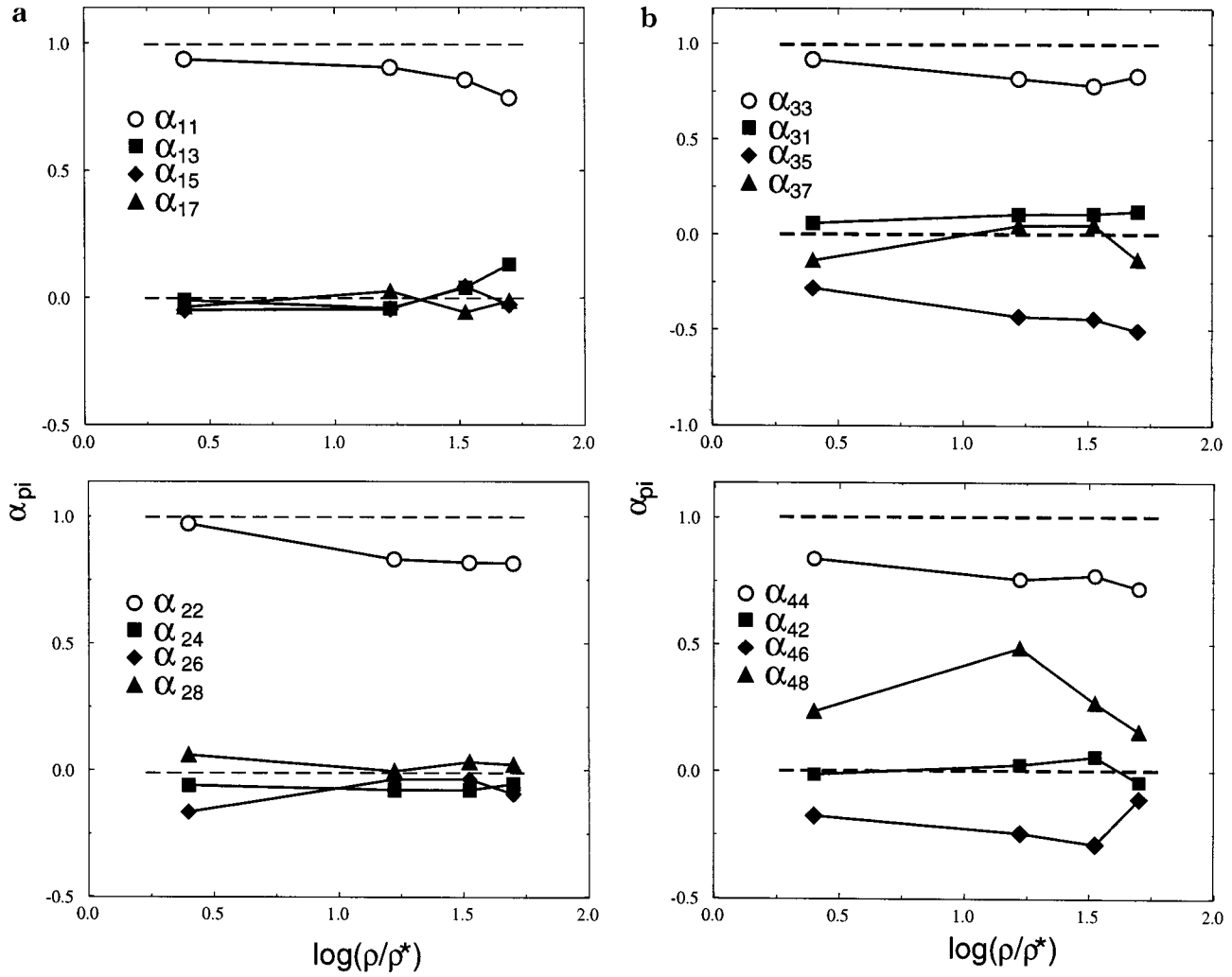

Figure 11. (a) Reduced density ρ/ρ^* dependence of expansion coefficients a_{pi} ($p = 1, 2$) computed from eq 15. Dashed lines are the predictions of the Rouse/reptation model. (b) Reduced density ρ/ρ^* dependence of expansion coefficients a_{pi} ($p = 3, 4$) computed from eq 15. Dashed lines are the predictions of the Rouse/reptation model.

The deviation of the simulation eigenfunctions from the theoretical prediction becomes more pronounced with increasing density and higher modes p. This is the behavior observed experimentally and can explain the broadening of the spectra with increasing density. It does not, however, provide any insight into the appearance of the secondary peak in the simulated spectra of dense systems.

A direct way to quantify the discrepancies between the theoretically predicted and the computed by simulations (integrated) eigenfunctions F_p is to expand F_p with respect to F_p^o as

$$F_p(n) = \sum_i a_{pi} F_i^o(n) \qquad (15)$$

and calculate the expansion coefficients a_{pi}. Computed coefficients are presented in Figures 11a and 11b. The dashed lines are the Rouse−Zimm model and the reptation model predictions for the diagonal ($a_{pp} = 1$) and the off-diagonal elements ($a_{pi} = 0$, $i \neq p$). Figures 11a and 11b demonstrate the discrepancy of the simulation coefficients from the theoretical predictions. For $p = 1$ the diagonal expansion coefficient decreases with ρ, whereas the rest of a_{pi} remains very close to the theoretical prediction. Increasing the density, this discrepancy becomes more important. For higher modes this behavior becomes increasingly pronounced.

From the above, it becomes evident that the eigenfunctions f_p progressively deviate from the model sinusoidal dependence on n. Therefore, we can identify more conclusively the reason of the spectra broadening with increasing density in terms of this deviation.

IV. Conclusions

Using equilibrium molecular dynamics trajectories, we have investigated the dielectric dynamic behavior of polymer chains. We established that the time autocorrelation functions of appropriate chain segments give information about the transient response of multi-inverted polar macromolecules under the influence of external electric fields. We obtained the dielectric spectra of polar chains symmetrically inverted λ times and the spectra of asymmetrically once-inverted chains. The dielectric loss curves of noninverted polar chains broaden considerably with density. For $\lambda \geq 1$ at a given density ρ, the spectra progressively reach the behavior of the Rouse model theoretical prediction. For asymmetrically once-inverted chains at a segment n^*, the spectra initially become more heterogeneous when moving n^* from 0 to the middle of the chains $N/2$. When n^* is close to $N/2$ the spectra have shapes close to the

noninverted ones, but shift to higher frequencies. Relaxation times τ_p ($p = 1-6$) were computed as the inverse of the maximum loss frequency. They exhibit a power-law dependence $\tau_p \propto p^{-\gamma}$ with $\gamma \simeq 2.08$. The ratio τ_p/τ_1 is independent of the density. This finding indicates that the span of relaxation times is not responsible for the dielectric loss spectra broadening. The reason for the broadening is identified by computing the eigenfunctions $f_p(n)$ of a local correlation function $C(n,t;m)$. These deviate from the Rouse−Zimm model and the reptation model prediction of a sinusoidal behavior ($f_p \propto \sin(p\pi n/N)$). The deviation becomes more pronounced with increasing density, resulting in broader relaxation spectra. Unfortunately, this analysis does not provide any insight into the secondary peak appearing at the high-frequency side of the simulation loss curves for dense systems of long chains. We do however express the optimism that simulations of longer than $N = 150$ chains could clearly reveal the relaxation mechanisms responsible for the secondary peak. The excellent agreement between the simulation and the experimental results clearly proves that the former can accurately capture the dynamic behavior of macromolecules.

Appendix

In this Appendix, we summarize the key features of the treatment of dipole-inverted chains, given by Watanabe et al.[5−7] Dipole-inverted polar chains have their dipoles parallel to the chain contour but inverted once at the n^*th segment. Hence, the dielectric relaxation process reflects the fluctuations of a vector $\Delta\mathbf{R}(t) = \mathbf{R}_1(t) - \mathbf{R}_2(t)$, where $\mathbf{R}_1$ and $\mathbf{R}_2$ are the vectors connecting the chain ends with the n^*th segment. The dielectric loss is now calculated by eq 1 with the correlation function given by

$$\phi_1(t,n^*) = \frac{1}{N}\left[\int_0^{n^*} \mathrm{d}n - \int_{n^*}^{N} \mathrm{d}n\right]\left[\int_0^{n^*} \mathrm{d}m - \int_{n^*}^{N} \mathrm{d}m\right] C(n,t;m) \quad \text{(A1)}$$

which yields

$$\epsilon''(\omega,n^*)/\Delta\epsilon = \sum_{p=1}^{N} g_p(n^*) \frac{\omega\tau_p}{1+\omega^2\tau_p^2} \quad \text{(A2)}$$

where

$$g_p(n^*) = \frac{2}{N^2}\left(\int_0^{n^*} f_p(n)\,\mathrm{d}n - \int_{n^*}^{N} f_p(n)\,\mathrm{d}n\right)^2 \quad \text{(A3)}$$

Watanabe and co-workers examined the dielectric response of dipole-inverted PI chains with various n^* values 0, n_1, n_2,...,$N/2$. From the dielectric loss curves of chains with $n^* = 0$ and $n^* = N/2$ they computed the relaxation times τ_1 and τ_2, respectively, as the inverse of the peak frequencies, and they tentatively estimated τ_3.[5] Using eq A2 they then obtained the intensities $g_p(n^*)$, using a least-squares fitting procedure, and were able to, in turn, estimate the eigenfunctions f_p (by differentiation), for several inversion positions n^*. Watanabe and co-workers[5−7] classified the odd eigenfunctions ($p = 1,3,..$) as symmetrical ($f_p(n) = f_p(N-n)$) and the even ones as asymmetrical ($f_p(n) = -f_p(N-n)$) with respect to the chain center ($n = N/2$), considering that the two ends move in an equivalent fashion. Then the integrals defined as

$$F_p(n^*) = \frac{\sqrt{2}}{N}\int_0^{n^*} f_p(n)\,\mathrm{d}n \quad \text{(A4)}$$

can be evaluated as

$$F_p(N/2) - F_p(n^*) = \pm[g_p(n^*)/4]^{1/2} (= 0 \text{ for } n^* = N/2);\ p = \text{odd} \quad \text{(A5)}$$

and

$$F_p(n^*) = \pm[g_p(n^*)/4]^{1/2} (= 0 \text{ for } n^* = 0);\ p = \text{even} \quad \text{(A6)}$$

satisfying the normalization relationship, $\sum_{p=1}^{N} F(n)F_p(m) = n/N$, for $n \le m$ and $= m/N$ when $n > m$.[5−7] This relationship corresponds to the initial condition $C(n,0;m) = \delta_{nm}$ for the local correlation function. Because, $f_p(n)$ and $-f_p(n)$ are equivalent eigenfunctions, one can choose either $+[g_p(n^*)/4]^{1/2}$ or $-[g_p(n^*)/4]^{1/2}$ for $n^* = 0$ in eq A5 and $n^* = n_1$ in eq A6. Watanabe et al. chose $+[g_p(n^*)/4]^{1/2}$ in their articles. After having measured the dielectric loss $\epsilon''/\Delta\epsilon$ and the dielectric relaxation times τ_p, for $p = 1-3$, they calculated the quantities

$$\Delta F_p(n^*) = F_p(n^*) - F_p(N/2) = -\frac{\sqrt{2}}{N}\int_{n^*}^{N/2} f_p(n)\,\mathrm{d}n \quad \text{(A7)}$$

using eqs A3−A6.[5] Subsequently, from $\Delta F_p(n)$ they were able to calculate the eigenfunctions f_p when necessary.

References and Notes

(1) Runt, J. P.; Fitzgerald, J. J. (eds.) *Dielectric Spectroscopy of Polymeric Materials*; American Chemical Society: Washington, DC, 1997.
(2) Hedvig, P. *Dielectric Spectroscopy of Polymers*; Adam Hilger: Bristol, England, 1977.
(3) Stockmayer, W. H. *Pure Appl. Chem.* **1967**, *15*, 539.
(4) Adachi, K.; Kotaka, T. *Prog. Polym. Sci.* **1993**, *18*, 585.
(5) Watanabe, H.; Urakawa, O.; Kotaka, T. *Macromolecules* **1993**, *26*, 5073.
(6) Watanabe, H.; Urakawa, O.; Kotaka, T. *Macromolecules* **1994**, *27*, 3525.
(7) Watanabe, H.; Yamada, H.; Urakawa, O. *Macromolecules* **1995**, *28*, 6443.
(8) Patel, S. S.; Takahashi, K. M. *Macromolecules* **1992**, *25*, 4382.
(9) Urakawa, O.; Adachi K.; Kotaka, T. *Macromolecules* **1993**, *26*, 2042.
(10) Rouse, P. E. *J. Chem. Phys.* **1953**, *21*, 1272.
(11) Zimm, B. H. *J. Chem Phys.* **1956**, *24*, 269.
(12) Doi, M.; Edwards, S. F. *The Theory of Polymer Dynamics*; Clarendon Press: Oxford, 1986.
(13) De Gennes, P. G. *Scaling Concepts in Polymer Physics*; Cornell University: Ithaca, NY, 1979.
(14) Urakawa, O.; Adachi, K.; Kotaka, T.; Takemoto, Y.; Yasuda, H. *Macromolecules* **1994**, *27*, 7410.
(15) Muthukumar, M. *Macromolecules* **1984**, *17*, 971.
(16) Flory, P. J. *Principles of Polymer Chemistry*; Cornell University: Ithaca, NY, 1953.
(17) Urakawa, O.; Watanabe, H. *Macromolecules* **1997**, *30*, 652.
(18) Kaznessis, Y. N.; Hill, D. A.; Maginn, E. J. *J. Chem. Phys.* **1998**, *109*, 5078.
(19) Kaznessis, Y. N.; Hill, D. A.; Maginn, E. J. *J. Chem. Phys.* **1999**, *111*, 1325.
(20) Kaznessis, Y. N.; Hill, D. A.; Maginn, E. J. *Macromolecules* **1999**, *32*, 1284.
(21) Kremer, K.; Grest, G. S. *J. Chem. Phys.* **1989**, *92*, 5057.

MA990680U